THE JOURNAL OF PHYSICAL CHEMISTRY C
A JOURNAL OF THE AMERICAN CHEMICAL SOCIETY

pubs.acs.org/JPCC
Article

Determining the Structure–Property Relationships of Quasi-Two-Dimensional Semiconductor Nanoplatelets

Arin R. Greenwood,[$] Sergio Mazzotti,[$] David J. Norris, and Giulia Galli*

Cite This: J. Phys. Chem. C 2021, 125, 4820–4827

Read Online

ACCESS | Metrics & More | Article Recommendations | Supporting Information

ABSTRACT: We report a theoretical study of CdSe nanoplatelets aimed at identifying the main factors determining their photophysical properties. Using atomic configurations optimized with density functional theory calculations, we computed quasiparticle and exciton binding energies of nanoplatelets with two to seven monolayers. We employed many body perturbation theory at the GW level and solved the Bethe-Salpeter equation to obtain absorption spectra and excitonic properties. Our results, which agree well with recent experiments, were then used to design a model that allows us to disentangle the effects of quantum confinement, strain induced by passivating ligands, and dielectric environment on the electronic properties of nanoplatelets. We found that, for the model to accurately reproduce our first principle results, it is critical to account for surface stress and consider a finite potential barrier and energy-dependent effective masses when describing quantum confinement. Our findings call into question previous assumptions on the validity of an infinite barrier to describe carrier confinement in nanoplatelets, suggesting that it may be possible to optimize interfacial charge transfer and extraction by appropriately choosing passivating ligands. The model developed here is generalizable to core–shell platelets and enables the description of system sizes not yet directly treatable by first-principles calculations.

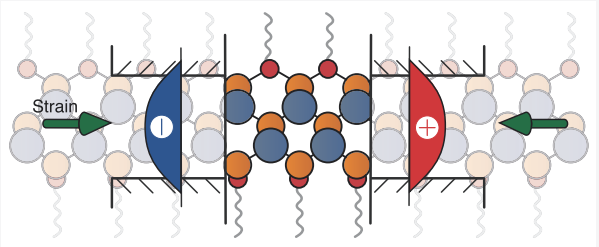

INTRODUCTION

Colloidal CdSe nanoplatelets (NPLs) are highly anisotropic, quasi-two-dimensional semiconductor nanostructures.[1,2] Much like epitaxially grown quantum wells, they exhibit optoelectronic properties that are governed by their tunable thickness of a few atomic layers. As a result, NPLs display absorption and emission line widths much narrower than spherical quantum dots (QDs). These optical properties make NPLs promising candidates as photoabsorbers in photovoltaic devices or in applications which require high color purity such as light-emitting diodes,[3] displays,[4] and lasers.[5]

At present, CdSe NPLs are routinely synthesized with passivating ligands that have been shown to affect their photophysical properties.[6,7] Consistent with computational reports,[8,9] experiments also suggest[6,7] that NPLs exhibit ligand-dependent strain profiles. However, a detailed understanding of the relationship between ligands, atomic structure, and photophysical properties is still missing. This is due, in part, to discrepancies between different computational methods adopted to model the properties of NPLs and interpret experiments, for example, their optical transition energies.[2,9−16]

In general, the optical gap (E_g) can be expressed as the difference between the quasiparticle (QP) gap E_{QP} (i.e., the difference between the ionization potential and electron affinity; also known as the fundamental gap) and the exciton binding energy, E_b. While optical transitions are routinely measured using, e.g., UV–vis spectroscopy, theoretically, E_g is most often obtained by computing E_{QP} and E_b separately. On the experimental side, an independent measure of quasiparticle and exciton binding energies is often challenging to obtain, particularly for nanoparticles and nanoplatelets in colloidal solutions, where photoemission measurements suffer from scattering due to the solvent. For colloidal NPLs, measurements of the QP energies have only recently become available,[16,17] through either photoacoustic[17] or scanning tunneling[16] spectroscopies. Due to the lack of data on QP and exciton binding energies, previous efforts have mostly compared theoretical results directly with optical transition energies. However, different methods were used to compute E_b and QP energies,[2,9−18] with results that differ significantly from each other, especially for the values of E_{QP}. Discrepancies between different methods may originate from both the level of theory adopted (e.g., effective-mass approximation, tight-binding, density functional theory (DFT) or many-body perturbation theory) and the choice of parameters (e.g., specific basis sets and pseudopotentials used in DFT calculations). Parametric discrepancies are easier to reconcile, while identifying the effects of theoretical assumptions on

Received: November 24, 2020
Revised: January 29, 2021
Published: February 17, 2021

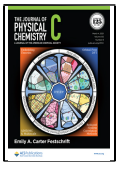

https://dx.doi.org/10.1021/acs.jpcc.0c10559
J. Phys. Chem. C 2021, 125, 4820–4827

computed properties is more challenging and has profound implications on our physical understanding of NPLs.

Here, we use a combination of first-principles calculations to rationalize how the photophysical properties of CdSe NPLs are affected by ligand-induced strain, quantum confinement, and dielectric contrast between the NPL and its environment. We focus on zincblende CdSe NPLs capped with atomic chloride ligands, as these are the simplest NPLs studied experimentally.[7,14,19] Using atomic configurations optimized with DFT calculations, we compute quasiparticle (QP) and exciton binding energies using Many Body Perturbation Theory at the G_0W_0 level and by solving the Bethe-Salpeter equation (BSE), respectively. Our results compare favorably with recent experimental reports[17] and are, to the best of our knowledge, the first calculations at this level of theory for NPLs. We then build a model of the quasiparticle gaps that reproduces our first-principles results. Such a model allows us to isolate the effects of quantum confinement, strain, and dielectric environment on the platelets' electronic properties. We show that to obtain good agreement between the model and first-principles descriptions of the NPLs, it is critical to account for surface stress effects and consider a finite, rather than infinite, potential barrier when describing quantum confinement. The model developed here not only allows one to disentangle the main effects determining the quasiparticle energies and hence optical gaps of the NPLs, but it also enables the description of system sizes not yet treatable directly by first-principles calculations. In addition, we show that the model can also be generalized to describe NPL heterostructures.

COMPUTATIONAL METHODS

We used Density Functional Theory (DFT) calculations to obtain structural models of chloride-passivated NPLs. DFT calculations were performed using the open-source plane-wave code Quantum Espresso[20] with the Perdew−Burke−Ernzerhof (PBE) exchange-correlation functional[21] and using Pseudo-Dojo pseudopotentials.[22] We used 2 × 2 × 1 supercells (28−68 atoms) with 3 × 3 × 1 k-points, allowing both the in-plane lattice constants and the atom positions to relax until forces were below 10^{-5} a.u.

G_0W_0 quasiparticle energies were calculated for the 2, 3, and 5 ML NPLs using the West code,[23] which does not require explicit calculation of empty states and avoids inversion of dielectric matrices. G_0W_0 calculations were performed on a primitive unit cell of 7−13 atoms for each NPL, using at least a 5 × 5 × 1 k-point mesh. G_0W_0 quasiparticle gaps were then extrapolated to infinite number of k-points in the lateral dimensions and to infinite number of projective dielectric eigenpotentials (PDEPs) to ensure converged results. The long-range Coulomb interaction was truncated to properly converge with respect to the vacuum spacing between periodic images in the axial direction, using the method discussed in ref.[24] We also showed that the G_0W_0 quasiparticle gap of the thinnest NPL (2 ML) obtained from the West[23] code was the same as that computed using the Yambo[25,26] code.

The exciton binding energy and absorption spectra of CdSe NPLs were calculated through the Bethe-Salpeter Equation (BSE) using the Yambo code[25,26] and using PBE wave functions and a scissor correction equal to the difference between the G_0W_0 and PBE gaps at the chosen k-point density for the 2 and 3 ML NPLs. The final spectrum for the 2 ML NPL was calculated with a 15 × 15 × 1 k-point mesh and includes transitions between 10 occupied and 10 unoccupied energy levels near the band edges. Exciton binding energies for the larger NPLs were extrapolated from smaller k-point densities. We provide thorough convergence studies in Section S1 of the SI and emphasize the importance of convergence with respect to the k-point mesh, as the BSE spectra were found to require a much denser mesh than that needed to converge PBE or G_0W_0 band gaps (see Section S1 in the SI for further details).

RESULTS AND DISCUSSION

We consider zincblende CdSe NPLs ranging between 2 and 7 monolayers (MLs) in thickness, where we define the number of monolayers to be equal to the number of layers of Se, adhering to the formula $Cd_{x+1}Se_x$, with Cd terminating both the top and bottom of the NPL. We chose NPLs capped with chloride ligands, as they have been successfully used in recent experiments,[7,14,19] with ligands initially placed as bridges between Cd atoms prior to structural relaxation.[27] Structures of 2, 3, 5, and 7 ML NPLs were then generated by fully relaxing all atomic positions and lattice constants using DFT calculations; we found that the relaxation of lattice constants in addition to atomic positions was essential to recover accurate strain profiles.

In Figure 1b,c, we show DFT results for the in-plane and out-of-plane strain for NPLs passivated with Cl^- and H^- (the latter results are from Zhou et al.,[9] who used the same level of theory as adopted here). We define the strain to be relative to the bulk lattice constant computed at the PBE level of theory. Consistent with previous reports,[6−9] our results show that NPLs are in a state of biaxial stress; they are subject to in-plane (ε_x) and out-of-plane (ε_z) strain, whose magnitude depends on the thickness and type of passivating ligands. We note in particular that different passivating ligands lead to different in- to out-of-plane strain ratios.

We analyze the strain observed in our first-principles calculations by using a continuum elastic model that includes surface stress (solid lines in Figure 1b,c), originally proposed for thin films.[28,29] The model shows that the in- and out-of-plane strain is determined by a subtle interplay between deformation energy of the bulk crystal, and surface stress (see Section S2 in the SI for details). We emphasize that neglecting the effect of the surface would not reproduce correctly our first-principles results. The model also rationalizes the observed overall contraction across all layers of c-ALD grown NPL heterostructures reported in recent experiments.[30]

We now turn to the electronic properties of the nanoplatelets, and we start by computing the quasiparticle energies of NPLs passivated with Cl^- ligands using the G_0W_0 approximation and PBE wave functions. Results are given in Figure 1d. G_0W_0 calculations were performed using the West code.[23] We did not include spin−orbit coupling (SOC) in our G_0W_0 calculations but expect SOC to lower the quasiparticle gaps by approximately 0.1 eV, as was found for bulk CdS G_0W_0 gaps in ref 31 as well as in our own PBE calculations of bulk CdSe.

We find the G_0W_0 quasiparticle gaps to be 3.52 eV for the 2 ML NPL, decreasing to 3.05 eV for the 3 ML NPL and to 2.43 eV for 5 ML. Our results are in good agreement with the only experimental reports of quasiparticle gaps for these materials,[16,17] as shown in Figure 1d. However, we note that the experimental samples were capped with carboxylate ligands and were measured either on a microscope coverslip[17] or Au

https://dx.doi.org/10.1021/acs.jpcc.0c10559
J. Phys. Chem. C 2021, 125, 4820−4827

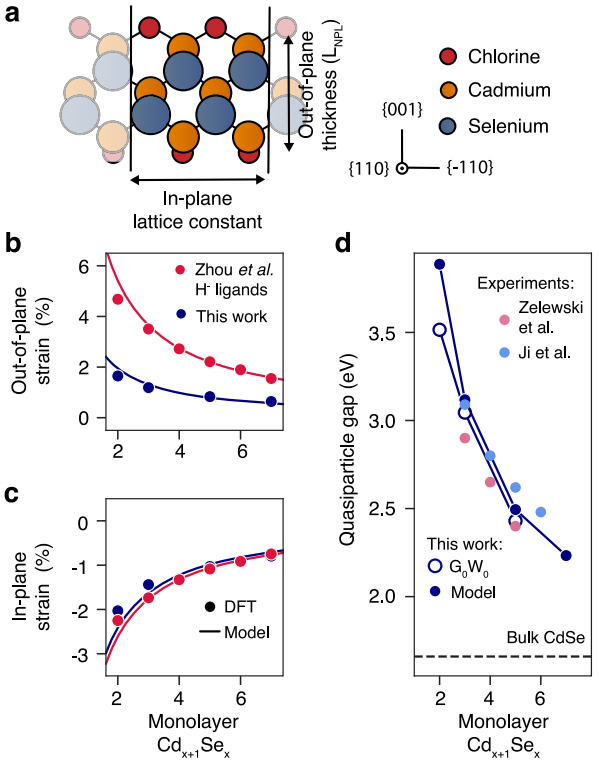

Figure 1. (a) Drawing of a 2 ML NPL labeling the in- and out-of-plane directions used throughout the text. (b) Out-of-plane and (c) in-plane strain as a percentage relative to the bulk lattice constant, for NPLs passivated with Cl^- ligands (blue) and H^- ligands, the latter using PBE data from Zhou et al.[9] Calculations were carried out at the DFT/PBE level of theory. Structural properties from DFT are analyzed using a continuum elastic model (red and blue solid lines). See text for details. (d) Quasiparticle gaps of CdSe NPLs calculated using G_0W_0 starting from PBE wave functions (empty blue circles), and estimated using the model described in the text (filled blue circles). Model and G_0W_0 results are compared to experimental data from photoacoustic[17] or scanning tunneling[16] spectroscopies.

substrate,[16] both with a dielectric constant different than that of vacuum.

To interpret our G_0W_0 calculations and extrapolate them to larger sizes, we developed a model aimed at disentangling three main effects: strain, quantum confinement, and dielectric contrast between the NPLs and their environment. We first consider the effect of strain using an eight-band **k·p**-Hamiltonian; we then compare two separate effective-mass models to estimate the change in gap due to quantum confinement. Finally, we describe the change of the gap as a function of the dielectric environment based on the results of ref 32. We mainly focus on the electron and heavy-hole energies, which are the states involved in the lowest optical transition energies in NPLs.[2]

We describe changes in the CdSe bulk band structure, and thus the band gap, as a function of strain using an effective mass **k·p**-Hamiltonian.[33] For zincblende crystals, such as CdSe, this Hamiltonian describes the energies of the electron, heavy (hh), and light-holes (lh), as well as the spin−orbit (SO) hole bands. At fixed momentum-vector k, the band-energies, and therefore also $E_{QP,bulk}$, are simply obtained by diagonalizing the **k·p**-Hamiltonian. Changes to the Γ-point energies of the heavy-hole and electron due to strain are given by[33]

$$\Delta E_e = a_p(1 - 2\eta)\varepsilon_z \quad (1)$$

$$\Delta E_{hh} = -a(1 - 2\eta)\varepsilon_z - b(1 + \eta)\varepsilon_z \quad (2)$$

where a, b, and a_p are the material-dependent deformation potentials. Out-of-plane (ε_z) and in-plane strain ($\varepsilon_y = \varepsilon_x$) are related through $\eta = -\varepsilon_x/\varepsilon_z$. The difference between electron and heavy-hole energy due to strain is then given as

$$\Delta E^{bulk}_{strain} = \Delta E_e - \Delta E_{hh} \quad (3)$$

In Figure 2a, we compare the pristine (unstrained) bulk band dispersion obtained from DFT calculations at the PBE

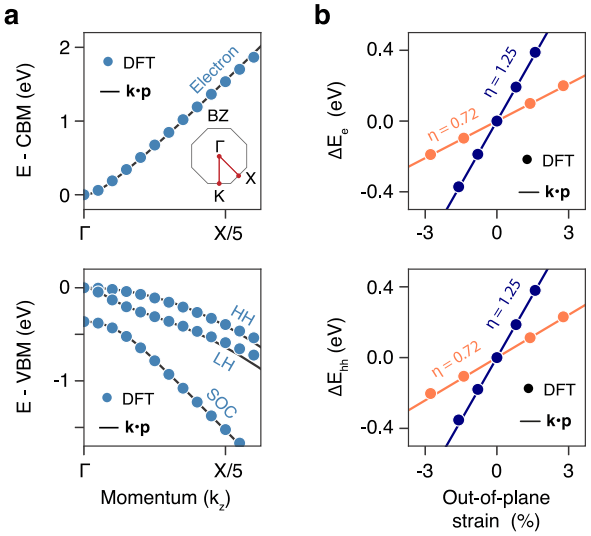

Figure 2. (a) Band structure of unstrained bulk CdSe, plotted as a function of the out-of-plane momentum (k_z), showing agreement between our DFT results (blue) and **k·p** model (solid lines). (b) The change in electron (top) and heavy-hole (bottom) energies of the bulk upon applied strain. The **k·p** model (orange solid lines) was parametrized using DFT data of strained bulk with a strain ratio of η = 0.72 (orange dots). The blue solid lines show predictions of the **k·p** model for a strain ratio of η = 1.25. See text for details. Model predictions agree well with DFT calculations that use η = 1.25 (blue dots).

level of theory to the results of the eight-band model which has been parametrized using our DFT results. We also plot the bulk Γ-point energies of both the heavy-hole and the electron, computed for different out-of-plane strains (Figure 2b). The deformation potentials (a, b, and a_p) were determined by using eqs 1 and 2 and by fitting DFT data obtained for the strained bulk, where the strain ratio was fixed to 0.72 (shown in orange). In a state of biaxial stress, η equals $C_{12}/(2C_{11})$[29] and therefore, the strain ratio of 0.72 is obtained using bulk elastic properties, C_{ij}.[34] The blue lines, in contrast, are an extrapolation of the model to η = 1.25, average strain-ratio in our Cl^- passivated NPLs, computed using the same deformation potentials. We compare the extrapolated model to DFT data of strained bulk with a fixed strain ratio of 1.25 (blue dots). The favorable comparison between the two indicates that the eight-band model accurately describes strain-induced changes in the electron and heavy-hole energies of the bulk, ΔE^{bulk}_{strain}.

To describe the effect of charge-carrier confinement ("quantum confinement"), we first consider an infinite potential-well that is often used in the literature to predict

https://dx.doi.org/10.1021/acs.jpcc.0c10559
J. Phys. Chem. C 2021, 125, 4820−4827

QP energies of NPLs.[2,11,12,16,18] The presence of infinite barriers forces the wave function (envelope) to vanish at the top and bottom of the NPL, thus leading to a discretization of the out-of-plane momentum ($k_z = n\pi/L_{NPL}$, n = 1,2,...). Most importantly, the smallest k_z is nonzero and increases with decreasing NPL thickness (L_{NPL}). In this case, we define the confinement energy, E_{conf}, as the difference between the band-energy at finite k_z obtained by diagonalizing the eight-band model and the respective Γ-point energies.

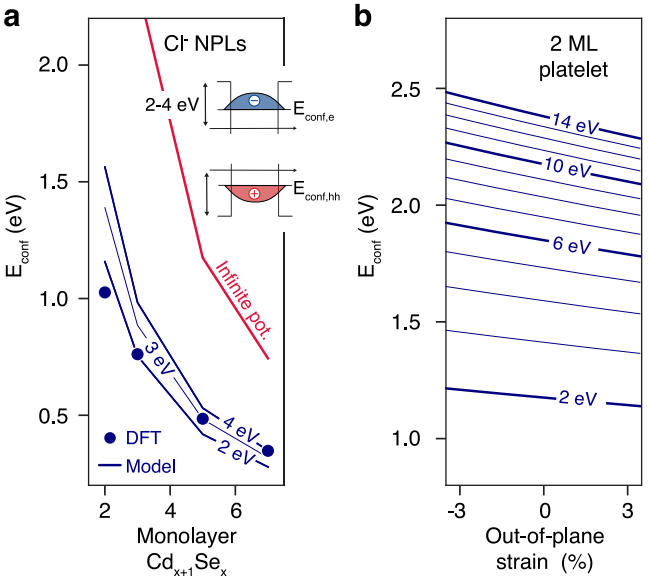

Figure 3. (a) Charge carrier confinement energy in NPLs; comparing the finite (blue) and infinite (red) potential-well models to DFT calculations of Cl^- passivated NPLs (blue dots). (b) Charge carrier confinement energy as a function of strain for the 2 ML NPL using increasing finite potentials between 2 and 14 eV. Results are computed by combining eq 3 and 4.

In Figure 3a, we show $E_{conf}^{DFT} = E_{NPL}^{DFT} - E_{bulk}^{DFT} - \Delta E_{strain}^{bulk}$, computed at the PBE level of theory for NPLs of different thickness and passivated with chloride ligands. Our DFT results for the confinement energy differ considerably from those obtained with a model assuming an infinite barrier; in particular, the infinite potential model strongly overestimates the PBE results, suggesting that the hypothesis of an infinite barrier needs to be revisited.

We thus modified the model by including the effect of a finite potential (V_0) on the confinement energy. For this purpose, heavy-hole (hh) and electron (e) are considered separately.[35] We approximate the heavy-hole dispersion assuming a constant effective mass [$m_{hh} = (\gamma_1 - 2\gamma_2)^{-1}$], where γ_i are the modified Luttinger parameters of the bulk.[33] To account for the nonparabolicity of the electron dispersion, we use an energy-dependent electron effective mass $m_e(E)$,[16,36,37] as this has proven to be effective in modeling confinement of electrons in epitaxial quantum wells with zincblende crystal structure[38] (see Section S3 in the SI for further details).

The heavy-hole ($E_{hh,conf}$) and electron ($E_{e,conf}$) confinement energies for a finite potential are then obtained by solving an implicit equation for $m_i = m_{hh}$ and $m_i = m_e(E_{e,conf})$, respectively,

$$\tan\left(\frac{L_{NPL}}{2}\sqrt{2m_iE_{i,conf}}\right) = \sqrt{m_i\left(\frac{V_0}{E_{i,conf}} - 1\right)} \quad (4)$$

Equation 4 is obtained by imposing continuity and current-conserving boundary conditions[39] for the wave function at both ends of the NPL. As done in models of quantum-dots[37] and NPLs,[17] a free-electron mass is assumed for heavy-hole and electron in the ligand shell and the vacuum region surrounding the NPLs. Strain-induced changes in the effective NPL-thickness are accounted for by L_{NPL}.

Figure 3b plots the confinement energy of a 2 ML-thick NPL as a function of out-of-plane strain, for different values of the confinement potential (V_0). Note that E_{conf} includes both $E_{e,conf}$ and $E_{hh,conf}$. Bulk parameters entering the model are extracted from DFT calculations which we carried out for the pristine and strained bulk. However, using experimental parameters for the bulk[2] yields similar results. We find that both out-of-plane strain and, to an even greater extent, V_0 remarkably affect the confinement energy. In Figure 3a, we show that it is only when considering a finite V_0, between 2 and 4 eV, that the model of eq 4, combined with changes in the electron and heavy-hole energies of the bulk due to strain (ΔE_{strain}^{bulk}, eq 3), agrees with our DFT calculations. These results call into question many literature assumptions of an infinite V_0.

We note that the strength of the confining potential is related to the extension of single particle wave functions associated with the platelet core, i.e., to their "leakage" into the ligand shell. Hence our results suggest that by using different passivating ligands, one may be able to optimize interfacial electronic coupling in NPLs and, therefore, engineer charge transfer and extraction.[40,41]

We also emphasize that since NPLs are only few monolayers thick, wave functions are strongly confined—even for V_0 of a few eVs—leading to quantized out-of-plane momenta (k_z) far from the Brioullin zone center. At these large momenta, the conduction band dispersion is nonparabolic (as shown in Figure 2a), and the assumption of parabolicity leads to significant errors when predicting the confinement energy. Although emphasized by Efros and co-workers,[2,16] this aspect has been largely neglected in the NPL modeling literature.[11,12,15,18] Using an energy-dependent electron effective mass[16,36−38] (as done in this work) is a simple but effective way to overcome the limitations of many current models of NPLs.

Having discussed quantum confinement, we now focus on how the dielectric environment affects the quasiparticle bandgap of NPLs. The quasiparticle gap measures the difference between ionization potential and electron affinity. In the presence of dielectric contrast, the creation of a hole in the valence band (ionization potential) or an electron in the conduction band (electron affinity) polarizes the interface between the NPL and the environment. This polarization, not present in the bulk, leads to a renormalization of the quasiparticle gap which can be described by the method of image charges[10,42] and accounted for by an additional self-energy, E_{self}. We compute E_{self} using the simple expression recently proposed by Cho et al.[32]

$$E_{self} = \frac{1}{\epsilon_{in}L_{NPL}}[2\tanh^{-1}(L_{12}) - \ln(1 - L_{12})] \quad (5)$$

https://dx.doi.org/10.1021/acs.jpcc.0c10559
J. Phys. Chem. C 2021, 125, 4820−4827

where L_{NPL} is the NPL thickness and $L_{12} = (\varepsilon_{in} - \varepsilon_{out})/(\varepsilon_{in} + \varepsilon_{out})$. ε_{in} and ε_{out} equal to the dielectric constant of the NPL and environment, respectively.

We are now in a position to combine the effects of strain, quantum confinement using a finite potential well model, and the self-energy due to the dielectric contrast to estimate the quasiparticle energy of NPLs, E_{NPL}^{QP}. We write the quasiparticle energy as

$$E_{NPL}^{QP} = E_{QP,bulk} + \Delta E_{strain}^{bulk} + E_{conf} + E_{self} \quad (6)$$

where ΔE_{strain}^{bulk}, E_{conf}, and E_{self} are defined as in eqs 3−5. A value of 2.5 eV for V_0 was assumed for all NPL thicknesses, as this was the average value found to best match our DFT data over the entire thickness range. It also corresponds to what has been used in the calculations for chloride-passivated NPLs by Christodoulou et al.[14] We further use our DFT calculations of NPLs to determine the strained NPL thickness (L_{NPL}), entering E_{conf} (eq 4) and E_{self} (eq 5), as well as the strain-profile entering ΔE_{strain}^{bulk} (eq 3). We take ε_{in} to be the bulk dielectric constant of CdSe (6.2), following Zhou et al.,[40] and assume ε_{out} to be that of vacuum. Finally, we use the experimental value of 1.66 eV for $E_{QP,bulk}$.[43] Further details can be found in the SI, Section S3.

In Figure 1d, we compare the quasiparticle gap computed using eq 6 to our G_0W_0 results and experimental reports.[16,17] The close agreement between the results of the model and our G_0W_0 calculations, as well as experimental reports, suggests that the quasiparticle gap is correctly described only when strain effects, dielectric contrast between NPL and environment, and charge-carrier confinement are all properly taken into account. For charge-carrier confinement, we emphasize the importance of considering both the presence of a finite (rather than infinite) barrier and accounting for electron effective masses that are not constant but rather dependent on the confinement-energy. The model for charge-carrier confinement presented here (eq 4) unifies both effects in a simple fashion.

Although derived and validated for "core-only" NPLs, eq 6 can be generalized to describe core−shell heterostructures, in particular, the ones grown using c-ALD techniques[30,44] that allow for shell-thickness control with monolayer precision. The presence of a shell affects the dielectric environment as well as the charge-carrier confinement, due to the band offset between core and shell. In addition, the difference between the lattice constant of core and shell causes core−shell NPLs to exhibit additional strain. As shown in the SI (Section S2.1), this can be accounted for by using a generalization of the continuum elastic model discussed above for core-only NPLs.

As a result, the shell affects ΔE_{strain}^{bulk}, E_{conf}, and E_{self} entering eq 6. Changes in the bulk band gap due to strain (ΔE_{strain}^{bulk}) and dielectric-contrast effects (E_{self}) can be incorporated using eq 3 and eq 5 (see Section S4 in the SI for further details). However, charge-carrier confinement in core−shell NPLs is determined by the interplay of multiple confining potentials and thus cannot be described using eq 4.

For simple core−shell systems, a core sandwiched between two shells of the same material and thickness, a closed form solution similar to the one in eq 4 exists. The confinement energy of either electron or hole is obtained by solving an implicit equation (see Section S3.1 in the SI for derivation)

$$\tan(k_0 z_1) = \gamma_{01}\frac{\tanh(k_1 d_1) + \gamma_{12}}{1 + \gamma_{12}\tanh(k_1 d_1)}; \quad \gamma_{ij} = \frac{m_i k_j}{m_j k_i} \quad (7)$$

Here, m_i is the effective mass of both electron and hole in the core (m_0) and shell (m_1) materials. Similarly to core-only NPLs, m_0 for electrons is energy-dependent. The effective mass of the ligand shell and environment is given by m_2. The core and shell thickness are $2z_0$ and d_1, respectively. V_1 describes the effect of the band offset and V_2 the confining potential due to the ligands (Figure 4a). In addition, $k_0 = \sqrt{2m_0 E_{conf}}$, while

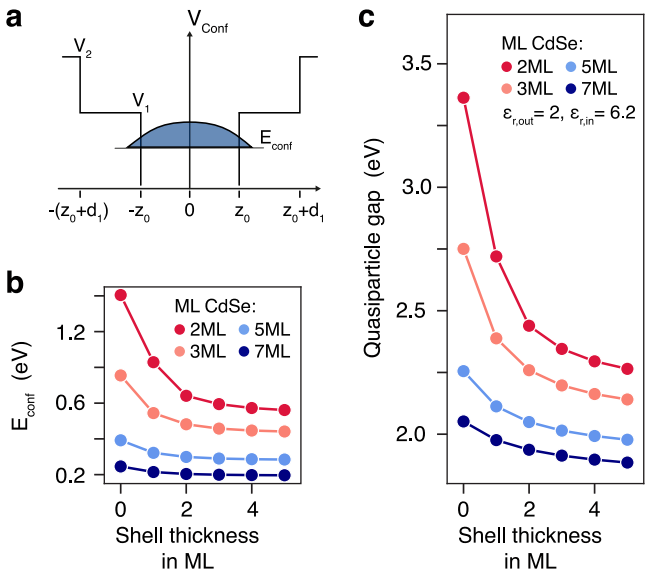

Figure 4. (a) Schematic of the confining potentials in core−shell NPLs. (b) Charge-carrier confinement energy, E_{conf}, and (c) quasiparticle gap as a function of shell thickness plotted for different NPL cores.

$k_i = \sqrt{2m_i(V_i - E_{conf})}$; $i = 1, 2$. Since all k_i depend on E_{conf}, eq 7 provides an implicit equation to evaluate the confinement energy in a core−shell NPL.

Using eq 7, in Figure 4b, we show the confinement energy, E_{conf}, in CdSe-core and CdS-shell NPLs for increasing shell thicknesses (see Section S4 in the SI for further details), where two limiting cases may be identified. For vanishing shell thickness, E_{conf} equals the result of core-only NPLs and is entirely dictated by the type of ligands. The confinement energy can then be computed using eq 4, with V_0 being the confinement potential of the ligands. For very thick (larger than ∼5 monolayers) shells, the effect of the ligands becomes irrelevant, and the confinement of the charge carriers is determined exclusively by the band-offset between the core and the shell. For all intermediate cases, the confinement energy is described by eq 7.

For vanishing shell thicknesses, charge carriers in the NPL core experience only the effect of the dielectric contrast between core and environment. Instead, for infinitely thick shells, the dielectric contrast is determined by the shell only. For simplicity, here, we assume that shell and core have approximately the same dielectric constant and in Figure 4c, we plot the quasiparticle gap in CdSe-core and CdS-shell NPLs for increasing shell thicknesses. Details on the calculations, including all information on the parameters used, can be found in the SI, Section S4. Our results show a saturation of the

https://dx.doi.org/10.1021/acs.jpcc.0c10559
J. Phys. Chem. C 2021, 125, 4820−4827

quasiparticle gap with increasing shell thickness, which is consistent with what has been shown experimentally for the optical gap.[30] The observed trends in E_{self} and E_{conf} intuitively explain the gap behavior.

In addition to rationalizing experimental results on core−shell heterostructures, eq 6 can be used to understand the changes in the quasiparticle energies of NPLs due to different ligands.[6,7] Passivating ligands have all similar dielectric constants (ε_{out}) of approximately two; therefore, differences in dielectric contrast due to ligands can be neglected. However, the biaxial strain due to surface stress and the barrier height (V_0) do vary as a function of the ligand type. The results of Figure 3b suggest the barrier height to be the dominant effect. These findings are consistent with a recent experimental report showing that differences between the optical gap of carboxylate and halide passivated NPLs cannot be explained considering stain-effects only.[7] However, for a quantitative comparison with measured optical gaps, $E_g = E_{QP} - E_b$, the evaluation of the exciton binding energy (E_b) is required, which we discuss next.

We compute the optical absorption spectra and exciton binding energy of NPLs using the Bethe-Salpeter equation, thus obtaining a direct calculation of E_b from first principles. We find the exciton binding energy of the 2 ML NPL to be approximately 600 meV, reducing to 500 eV for 3 ML. In Figure 5a, we show the absorption spectrum of 2 ML CdSe calculated by solving the BSE starting from PBE wave functions, with a constant scissor correction equal to the difference between the quasiparticle gaps obtained at the PBE and G_0W_0 levels of theory. Our BSE calculations explicitly included spin−orbit coupling, as qualitative agreement with experimental absorption spectra, shown in Figure 5a, could not otherwise be obtained because the first two peaks originate from transitions of the heavy- and light-hole.[2]

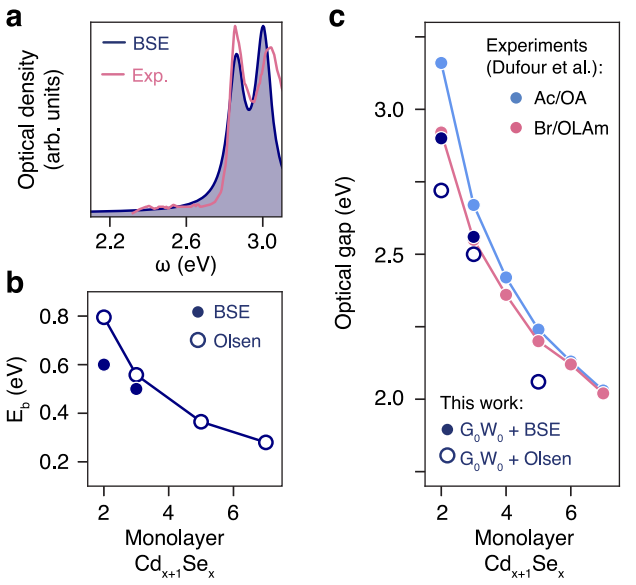

Figure 5. (a) Qualitative comparison between the BSE spectrum of a 2 ML NPL and experimental data from ref 2. The experimental spectra is shifted to match the optical gap of BSE. The BSE spectrum was calculated using 15 × 15 × 1 k-point sampling and is plotted with a Lorentzian broadening of 0.05 eV. (b) Exciton binding energies calculated using BSE (filled blue circles) and the Olsen model[45] (empty blue circles). (c) Quantitative comparison of our calculated optical gaps [either G_0W_0 and BSE (filled blue circles), or G_0W_0 and Olsen's model (empty blue circles)] with experimental results[7] of NPLs passivated either with acetate and oleate (Ac/OA), or bromide and oleylamine (Br/OLAm) ligands.

Besides providing a value for the exciton binding energy for Cl^- passivated NPLs in vacuum, BSE calculations can help asses the validity of models presented in the literature. While most calculations use the bulk exciton reduced-mass (μ), our DFT calculations of NPLs, in line with the report by Benchamekh et al.,[10] suggest that μ differs substantially from the bulk value due to confinement[38,39] and strain.[33]

Comparison between Olsen's 2D Screened Hydrogen model[45] and BSE calculations (Figure 5b, empty and filled blue circles, respectively) shows that Olsen's model, where a 2D polarizability is the fundamental variable, overestimates our BSE results for the 2 and 3 ML NPLs, with better agreement for the thicker 3 ML NPL. For further details, see Section S1 in the SI. These findings are consistent with the observation[45] that the model performs best for exciton binding energies below approximately 500 meV. A direct comparison between our first principle results and other exciton models proposed in the literature, including both purely 2D[9] and hybrid,[10] is not straightforward, due to the use of dielectric constants $\varepsilon_{r,out}$ of 2 instead of 1 (vacuum), as intrinsically assumed in our BSE calculations. Exciton binding energies calculated with $\varepsilon_{r,out} \simeq 2$ instead of 1 are expected to be smaller[10,32,46] than those obtained in this work.

Having computed the G_0W_0 quasiparticle gap and exciton binding energy, we finally compare our calculated optical gaps with experimental results[7] of NPLs passivated either with acetate and oleate (Ac/OA), or bromide and oleylamine (Br/OLAm) ligands. The latter (Br/OLAm) have been shown to exhibit optical gaps similar to chloride and oleylamine passivated NPLs. The same has been observed for wurtzite CdSe NPLs.[47,48] Indeed, we find good agreement with BSE and the Olsen model, especially when comparing to the experimental results for Br/OLAm-passivated NPLs (Figure 5c). Note that all our calculations assume vacuum ($\varepsilon_{r,out} = 1$), while the dielectric constant for the experimental environment is more likely to be 2. However, while the E_b and quasiparticle band gap are affected by changes in dielectric constant between the material and its environment, the optical band gap may be less sensitive to these changes.[10,32] The agreement between G_0W_0 combined to BSE ($\varepsilon_{r,out} = 1$) and experiments ($\varepsilon_{r,out} \simeq 2$) supports these observations; it suggests that the E_b and quasiparticle gap are affected by changes in dielectric contrast in opposite ways but by similar amounts.

CONCLUSIONS

We have presented first-principles results for the quasiparticle gap and exciton binding energy of a series of CdSe NPLs, as obtained from G_0W_0 and BSE calculations, respectively. Our G_0W_0 results are in good agreement with recent experimental reports, and, when combined with exciton binding energies obtained by solving the BSE, lead to optical gaps that compare favorably with experiment. To rationalize our calculations of the quasiparticle gap, we have presented a simple model that allows one to disentangle the effects of ligand-induced biaxial strain, quantum confinement, and the dielectric contrast between a NPL and its environment. We found that all three effects play a key role in determining the quasiparticle gap in NPLs. Importantly, we showed that the quasiparticle gap in NPLs is correctly described only when quantum confinement is modeled by a finite (rather than infinite) potential barrier

https://dx.doi.org/10.1021/acs.jpcc.0c10559
J. Phys. Chem. C 2021, 125, 4820−4827

and when an energy-dependent (rather than constant) effective mass is considered for the electron. These findings not only challenge current modeling assumptions but also imply that single particle wave functions exhibit a "leakage" into the ligand shell. In turn, our results suggest that tuning of the confinement potential, e.g., by using different passivating ligands, could be an effective approach to engineer interfacial coupling in NPLs.

The model presented here is not limited to CdSe NPLs, but it can be applied to any quasi-two-dimensional nanocrystal with a zincblende crystal structure. Due to its much-reduced computational cost relative to G_0W_0 calculations, this model can be easily used to predict the quasiparticle gaps of systems that are too computationally demanding for first-principles calculations, including the description of NPL heterostructures.

■ ASSOCIATED CONTENT

Supporting Information

The Supporting Information is available free of charge at https://pubs.acs.org/doi/10.1021/acs.jpcc.0c10559.

Computational details on DFT, G_0W_0, and BSE calculations, and derivations of continuum elastic models as well as finite potential well models for core-only and core−shell NPLs, respectively (PDF)

All structures of strained and unstrained bulk CdSe as well as the CdSe NPLs studied in this work (ZIP)

■ AUTHOR INFORMATION

Corresponding Author

Giulia Galli − *Pritzker School of Molecular Engineering, University of Chicago, Chicago, Illinois 60637, United States; Department of Chemistry, University of Chicago, Chicago, Illinois 60637, United States; Argonne National Laboratory, Argonne, Illinois 60439, United States;* orcid.org/0000-0002-8001-5290; Email: gagalli@uchicago.edu

Authors

Arin R. Greenwood − *Pritzker School of Molecular Engineering, University of Chicago, Chicago, Illinois 60637, United States;* orcid.org/0000-0002-5593-9301

Sergio Mazzotti − *Optical Materials Engineering Laboratory, Department of Mechanical and Process Engineering, ETH Zurich, Zurich 8092, Switzerland;* orcid.org/0000-0001-6314-9580

David J. Norris − *Optical Materials Engineering Laboratory, Department of Mechanical and Process Engineering, ETH Zurich, Zurich 8092, Switzerland;* orcid.org/0000-0002-3765-0678

Complete contact information is available at: https://pubs.acs.org/10.1021/acs.jpcc.0c10559

Author Contributions

[$]A.R.G. and S.M. contributed equally and are listed alphabetically.

Notes

The authors declare no competing financial interest.

■ ACKNOWLEDGMENTS

This work was supported by the U.S. Department of Energy, Office of Science, Basic Energy Sciences, Materials Sciences, and Engineering Division under contract number DE-SC0012405, and by MICCoM, as part of the Computational Materials Sciences Program funded by the U.S. Department of Energy, and by the Swiss National Science Foundation (SNSF) under Award No. 200021-188593. The authors thank F. Antolinez, A. Cocina, T. Francese, M. Govoni, F. Gygi, R. Keitel, P. Kumar, N. Lassaline, C. Lightner, A. Mule, A. Pun, V. Rozsa, M. Rusishvili, D Talapin, and H. Yang for insightful discussions.

■ REFERENCES

(1) Ithurria, S.; Dubertret, B. Quasi 2D Colloidal CdSe Platelets with Thicknesses Controlled at the Atomic Level. *J. Am. Chem. Soc.* **2008**, *130*, 16504−16505.

(2) Ithurria, S.; Tessier, M.; Mahler, B.; Lobo, R.; Dubertret, B.; Efros, Al. L. Colloidal Nanoplatelets with Two-Dimensional Electronic Structure. *Nat. Mater.* **2011**, *10*, 936−941.

(3) Chen, Z.; Nadal, B.; Mahler, B.; Aubin, H.; Dubertret, B. Quasi-2D Colloidal Semiconductor Nanoplatelets for Narrow Electroluminescence. *Adv. Funct. Mater.* **2014**, *24*, 295−302.

(4) Cunningham, P. D.; Souza, J. B., Jr.; Fedin, I.; She, C.; Lee, B.; Talapin, D. V. Assessment of Anisotropic Semiconductor Nanorod and Nanoplatelet Heterostructures with Polarized Emission for Liquid Crystal Display Technology. *ACS Nano* **2016**, *10*, 5769−5781.

(5) Grim, J. Q.; Christodoulou, S.; Di Stasio, F.; Krahne, R.; Cingolani, R.; Manna, L.; Moreels, I. Continuous-Wave Biexciton Lasing at Room Temperature Using Solution-Processed Quantum Wells. *Nat. Nanotechnol.* **2014**, *9*, 891−895.

(6) Antanovich, A.; Achtstein, A.; Matsukovich, A.; Prudnikau, A.; Bhaskar, P.; Gurin, V.; Molinari, M.; Artemyev, M. A Strain-Induced Exciton Transition Energy Shift in CdSe Nanoplatelets: The Impact of an Organic Ligand Shell. *Nanoscale* **2017**, *9*, 18042−18053.

(7) Dufour, M.; Qu, J.; Gréboval, C.; Méthivier, C.; Lhuillier, E.; Ithurria, S. Halide Ligands to Release Strain in Cadmium Chalcogenide Nanoplatelets and Achieve High Brightness. *ACS Nano* **2019**, *13*, 5326−5334.

(8) Vasiliev, R. B.; Lebedev, A. I.; Lazareva, E. P.; Shlenskaya, N. N.; Zaytsev, V. B.; Vitukhnovsky, A. G.; Yao, Y.; Sakoda, K. High-Energy Exciton Transitions in Quasi-Two-Dimensional Cadmium Chalcogenide Nanoplatelets. *Phys. Rev. B: Condens. Matter Mater. Phys.* **2017**, *95*, 165414.

(9) Zhou, Q.; Cho, Y.; Yang, S.; Weiss, E. A.; Berkelbach, T. C.; Darancet, P. Large Band Edge Tunability in Colloidal Nanoplatelets. *Nano Lett.* **2019**, *19*, 7124−7129.

(10) Benchamekh, R.; Gippius, N. A.; Even, J.; Nestoklon, M.; Jancu, J.-M.; Ithurria, S.; Dubertret, B.; Efros, Al. L.; Voisin, P. Tight-Binding Calculations of Image-Charge Effects in Colloidal Nanoscale Platelets of Cdse. *Phys. Rev. B: Condens. Matter Mater. Phys.* **2014**, *89*, 035307.

(11) Rajadell, F.; Climente, J. I.; Planelles, J. Excitons in Core-Only, Core-Shell and Core-Crown CdSe Nanoplatelets: Interplay between In-Plane Electron-Hole Correlation, Spatial Confinement, and Dielectric Confinement. *Phys. Rev. B: Condens. Matter Mater. Phys.* **2017**, *96*, 035307.

(12) Planelles, J. Simple Correlated Wave-Function for Excitons in 0D, Quasi-1D and Quasi-2D Quantum Dots. *Theor. Chem. Acc.* **2017**, *136*, 81.

(13) Planelles, J.; Achtstein, A. W.; Scott, R.; Owschimikow, N.; Woggon, U.; Climente, J. I. Tuning Intraband and Interband Transition Rates via Excitonic Correlation in Low-Dimensional Semiconductors. *ACS Photonics* **2018**, *5*, 3680−3688.

(14) Christodoulou, S.; Climente, J. I.; Planelles, J.; Brescia, R.; Prato, M.; Martín-García, B.; Khan, A. H.; Moreels, I. Chloride-Induced Thickness Control in CdSe Nanoplatelets. *Nano Lett.* **2018**, *18*, 6248−6254.

(15) Llusar, J.; Planelles, J.; Climente, J. I. Strain in Lattice-Mismatched CdSe-Based Core/Shell Nanoplatelets. *J. Phys. Chem. C* **2019**, *123*, 21299−21306.

(16) Ji, B.; Rabani, E.; Efros, Al. L.; Vaxenburg, R.; Ashkenazi, O.; Azulay, D.; Banin, U.; Millo, O. Dielectric Confinement and Excitonic

Effects in Two-Dimensional Nanoplatelets. *ACS Nano* **2020**, *14*, 8257−8265.
(17) Zelewski, S. J.; Nawrot, K. C.; Zak, A.; Gladysiewicz, M.; Nyk, M.; Kudrawiec, R. Exciton Binding Energy of Two-Dimensional Highly Luminescent Colloidal Nanostructures Determined from Combined Optical and Photoacoustic Spectroscopies. *J. Phys. Chem. Lett.* **2019**, *10*, 3459−3464.
(18) Shornikova, E. V.; Biadala, L.; Yakovlev, D. R.; Sapega, V. F.; Kusrayev, Y. G.; Mitioglu, A. A.; Ballottin, M. V.; Christianen, P. C.; Belykh, V. V.; Kochiev, M. V.; et al. Addressing the Exciton Fine Structure in Colloidal Nanocrystals: The Case of CdSe Nanoplatelets. *Nanoscale* **2018**, *10*, 646−656.
(19) Cho, W.; Kim, S.; Coropceanu, I.; Srivastava, V.; Diroll, B. T.; Hazarika, A.; Fedin, I.; Galli, G.; Schaller, R. D.; Talapin, D. V. Direct Synthesis of Six-Monolayer (1.9 nm) Thick Zinc-Blende CdSe Nanoplatelets Emitting at 585 nm. *Chem. Mater.* **2018**, *30*, 6957−6960.
(20) Giannozzi, P.; Baroni, S.; Bonini, N.; Calandra, M.; Car, R.; Cavazzoni, C.; Ceresoli, D.; Chiarotti, G. L.; Cococcioni, M.; Dabo, I.; et al. QUANTUM ESPRESSO: A Modular and Open-Source Software Project for Quantum Simulations of Materials. *J. Phys.: Condens. Matter* **2009**, *21*, 395502.
(21) Perdew, J. P.; Burke, K.; Ernzerhof, M. Generalized Gradient Approximation Made Simple. *Phys. Rev. Lett.* **1996**, *77*, 3865−3868.
(22) van Setten, M. J.; Giantomassi, M.; Bousquet, E.; Verstraete, M. J.; Hamann, D. R.; Gonze, X.; Rignanese, G.-M. The PseudoDojo: Training and Grading a 85 Element Optimized Norm-Conserving Pseudopotential Table. *Comput. Phys. Commun.* **2018**, *226*, 39−54.
(23) Govoni, M.; Galli, G. Large Scale GW Calculations. *J. Chem. Theory Comput.* **2015**, *11*, 2680−2696.
(24) Smart, T. J.; Wu, F.; Govoni, M.; Ping, Y. Fundamental Principles for Calculating Charged Defect Ionization Energies in Ultrathin Two-Dimensional Materials. *Phys. Rev. Mater.* **2018**, *2*, 124002.
(25) Sangalli, D.; Ferretti, A.; Miranda, H.; Attaccalite, C.; Marri, I.; Cannuccia, E.; Melo, P. M.; Marsili, M.; Paleari, F.; Marrazzo, A.; et al. Many-Body Perturbation Theory Calculations Using the Yambo Code. *J. Phys.: Condens. Matter* **2019**, *31*, 325902.
(26) Marini, A.; Hogan, C.; Gruning, M.; Varsano, D. An Ab Initio Tool for Excited State Calculations. *Comput. Phys. Commun.* **2009**, *180*, 1392−1403.
(27) Szemjonov, A.; Pauporté, T.; Ithurria, S.; Lequeux, N.; Dubertret, B.; Ciofini, I.; Labat, F. Ligand-Stabilized CdSe Nanoplatelet Hybrid Structures with Tailored Geometric and Electronic Properties. New Insights from Theory. *RSC Adv.* **2014**, *4*, 55980−55989.
(28) Gurtin, M. E.; Murdoch, A. I. Surface Stress in Solids. *Int. J. Solids Struct.* **1978**, *14*, 431−440.
(29) Streitz, F. H.; Cammarata, R. C.; Sieradzki, K. Surface-Stress Effects on Elastic Properties. I. Thin Metal Films. *Phys. Rev. B: Condens. Matter Mater. Phys.* **1994**, *49*, 10699.
(30) Hazarika, A.; Fedin, I.; Hong, L.; Guo, J.; Srivastava, V.; Cho, W.; Coropceanu, I.; Portner, J.; Diroll, B. T.; Philbin, J. P.; et al. Colloidal Atomic Layer Deposition with Stationary Reactant Phases Enables Precise Synthesis of "Digital" II−VI Nano-Heterostructures with Exquisite Control of Confinement and Strain. *J. Am. Chem. Soc.* **2019**, *141*, 13487−13496.
(31) Scherpelz, P.; Govoni, M.; Hamada, I.; Galli, G. Implementation and Validation of Fully Relativistic GW Calculations: Spin−Orbit Coupling in Molecules, Nanocrystals, and Solids. *J. Chem. Theory Comput.* **2016**, *12*, 3523−3544.
(32) Cho, Y.; Berkelbach, T. C. Environmentally Sensitive Theory of Electronic and Optical Transitions in Atomically Thin Semiconductors. *Phys. Rev. B: Condens. Matter Mater. Phys.* **2018**, *97*, 041409.
(33) Bahder, T. B. Eight-Band k·p Model of Strained Zinc-Blende Crystals. *Phys. Rev. B: Condens. Matter Mater. Phys.* **1990**, *41*, 11992.
(34) Ouendadji, S.; Ghemid, S.; Meradji, H.; Hassan, F. E. H. Theoretical Study of Structural, Electronic, and Thermal Properties of CdS, CdSe and CdTe Compounds. *Comput. Mater. Sci.* **2011**, *50*, 1460−1466.
(35) Schuurmans, M.; t' Hooft, G. W. Simple Calculations of Confinement States in a Quantum Well. *Phys. Rev. B: Condens. Matter Mater. Phys.* **1985**, *31*, 8041.
(36) Ekimov, A. I.; Hache, F.; Schanne-Klein, M. a.; Ricard, D.; Flytzanis, C.; Kudryavtsev, I.; Yazeva, T.; Rodina, A.; Efros, Al. L. Absorption and Intensity-Dependent Photoluminescence Measurements on CdSe Quantum Dots: Assignment of the First Electronic Transitions. *J. Opt. Soc. Am. B* **1993**, *10*, 100−107.
(37) Norris, D. J.; Bawendi, M. Measurement and Assignment of the Size-Dependent Optical Spectrum in CdSe Quantum Dots. *Phys. Rev. B: Condens. Matter Mater. Phys.* **1996**, *53*, 16338.
(38) Wetzel, C.; Efros, Al. L.; Moll, A.; Meyer, B.; Omling, P.; Sobkowicz, P. Dependence on Quantum Confinement of the In-Plane Effective Mass in $Ga_{0.47}In_{0.53}As$/InP Quantum Wells. *Phys. Rev. B: Condens. Matter Mater. Phys.* **1992**, *45*, 14052.
(39) Yu, P. Y.; Cardona, M. *Fundamentals of Semiconductors*, 3rd ed.; Springer: Berlin, 2001; pp 479−488.
(40) Zhu, H.; Song, N.; Lian, T. Controlling Charge Separation and Recombination Rates in CdSe/ZnS Type I Core-Shell Quantum Dots by Shell Thicknesses. *J. Am. Chem. Soc.* **2010**, *132*, 15038−15045.
(41) Tisdale, W. A.; Zhu, X. Y. Artificial Atoms on Semiconductor Surfaces. *Proc. Natl. Acad. Sci. U. S. A.* **2011**, *108*, 965−970.
(42) Kumagai, M.; Takagahara, T. Excitonic and Nonlinear-Optical Properties of Dielectric Quantum-Well Structures. *Phys. Rev. B: Condens. Matter Mater. Phys.* **1989**, *40*, 12359.
(43) Kim, Y. D.; Klein, M. V.; Ren, S. F.; Chang, Y.; Luo, H.; Samarth, N.; Furdyna, J. K. Optical Properties of Zinc-Blende CdSe and $Zn_xCd_{1-x}Se$ Films Grown on GaAs. *Phys. Rev. B: Condens. Matter Mater. Phys.* **1994**, *49*, 7262−7270.
(44) Ithurria, S.; Talapin, D. V. Colloidal Atomic Layer Deposition (c-ALD) using Self-Limiting Reactions at Nanocrystal Surface Coupled to Phase Transfer between Polar and Nonpolar Media. *J. Am. Chem. Soc.* **2012**, *134*, 18585−18590.
(45) Olsen, T.; Latini, S.; Rasmussen, F.; Thygesen, K. S. Simple Screened Hydrogen Model of Excitons in Two-Dimensional Materials. *Phys. Rev. Lett.* **2016**, *116*, 056401.
(46) Achtstein, A. W.; Schliwa, A.; Prudnikau, A.; Hardzei, M.; Artemyev, M. V.; Thomsen, C.; Woggon, U. Electronic Structure and Exciton-Phonon Interaction in Two-Dimensional Colloidal CdSe Nanosheets. *Nano Lett.* **2012**, *12*, 3151−3157.
(47) Zhou, Y.; Buhro, W. E. Reversible Exchange of L-Type and Bound-Ion-Pair X-Type Ligation on Cadmium Selenide Quantum Belts. *J. Am. Chem. Soc.* **2017**, *139*, 12887−12890.
(48) Yao, Y.; Zhou, Y.; Sanderson, W. M.; Loomis, R. A.; Buhro, W. E. Metal-Halide-Ligated Cadmium Selenide Quantum Belts by Facile Surface Exchange. *Chem. Mater.* **2018**, *30*, 2848−2857.

https://dx.doi.org/10.1021/acs.jpcc.0c10559
J. Phys. Chem. C 2021, 125, 4820−4827